A general algorithm for the linear and quadratic gradients of physical quantities based on 10 or more point measurements

Chao Shen[1], Yufei Zhou[1], Yonghui Ma[1], Xiaogang Wang[2], Zuyin Pu[3], M. Dunlop[4, 5]

[1]School of Science, Harbin Institute of Technology, Shenzhen, 518055, China

[2]School of Physics, Harbin Institute of Technology, Harbin, 150001, China

[3]School of Earth and Space Sciences, Peking University, Beijing, China

[4]School of Space and Environment, Beihang University, Beijing, China

[5]Rutherford Appleton Laboratory, Chilton, DIDCOT, Oxfordshire OX11 0QX, United Kingdom

Key Points:

A general algorithm for the linear and quadratic gradients based on 10 or more spacecraft measurements is presented for the first time

The characteristic matrix of the constellation affecting the determination of the quadratic gradient has been found and its features shown

The algorithm has been tested on the magnetic field, indicating the obtained linear magnetic gradient is of second order accuracy

Abstract

In this study, a novel algorithm for jointly estimating the linear and quadratic gradients of physical quantities with multiple spacecraft observations based on the least square method has been put forward for the first time. With 10 or more spacecraft constellation measurements as the input, this new algorithm can yield both the linear and quadratic gradients at the barycenter of the constellation. Iterations have been used in the algorithm. The tests on cylindrical flux ropes, dipole magnetic field and modeled geo-magnetospheric field have been carried out. The tests indicate that the linear gradient gained has the second order accuracy, while the quadratic gradient is of the first order accuracy. The test on the modeled geo-magnetospheric field shows that, the more the number of the spacecraft in the constellation, the high the accuracy of the quadratic gradient calculated. However, the accuracy of the linear gradient yielded is independent of the number of the spacecraft. The feasibility, reliability and accuracy of this algorithm have been verified successfully. This algorithm can find wide applications in the design of the future multiple S/C missions as well as in the analysis of multiple point measurement data.

Plain Language Summary

With the development of space explorations, the constellations with 10 or more spacecraft may become true in the near future. However, there is still no general algorithm available for calculating the quadratic gradient of various physical quantities with 10 or more point measurements. In this article, we present a universal approach that can estimate both the linear and quadratic gradients of physical quantities based on 10 or more point measurements. This algorithm has been tested and its reliability has been verified. The tests show that the linear gradient obtained is of the second order accuracy, while the quadratic gradient the first order accuracy. This algorithm developed will be beneficial for the design of the future multiple S/C constellation missions and have wide applications in analyzing multiple point measurement data.

Key Words:

Multiple Spacecraft Measurements, Iteration, Linear gradient, Quadratic Gradient, Geometry of Magnetic Field Lines

1. Introduction

The gradients of physical quantities play important roles in the dynamic evolution of space plasmas. For example, the first-order gradient of electromagnetic fields balance their temporal variations as well as the sources (charge density and current density); the linear gradient of physical quantities (magnetic field, thermal pressure, etc.) can also drive the drift motions of the charged particles in electromagnetic fields. The linear gradient of physical quantities can be estimated from the 4 points in situ measurements with a first-order accuracy, and a lot of estimators have been developed already (Dunlop et al., 1988; Harvey, 1998; Chanteur, 1998; De Keyser, et al., 2007; Vogt et al., 2008; Vogt et al., 2009).

On the other hand, the quadratic gradient of physical quantities can lead to the diffusion and dissipation processes in plasmas. The quadratic gradients of electromagnetic potentials can balance the sources as shown by the Poisson equation. The geometry of the magnetic field depends on both the first order and the second-order magnetic gradients (Shen et al., 2020).

Recently some investigations have been made to fit the magnetic field to the second order based on the four spacecraft magnetic and current density observations (Torbert et al., 2020). Shen et al. (2020) have put forward an explicit algorithm to calculate the quadratic magnetic gradient as well as the complete geometry of magnetic field lines with 4 point magnetic field and particle/current density measurements under the constraints of electromagnetic laws. This approach, however, can not be applied to estimate the quadratic gradient of other physical fields, such as those of the density, temperature, and electric potential, etc. Generally, at least 10 point measurements of a physical quantity are required to calculate its second-order gradient (Chanteur, 1998).

With the development of space exploration, the constellation mission with 10 or more spacecraft has become possible (e.g., Cross-Scale mission). However, we still have no applicable universal algorithm for estimating the quadratic gradient of physical quantities with 10 and more point measurements.

In this paper, we present a universal algorithm that can estimate both the linear and quadratic gradients of physical quantities based on 10 or more point measurements. This algorithm has been tested and its reliability has been verified. The accuracy of this algorithm has been investigated. The algorithm is presented in the Section 2, the tests on the method have been made in Section 3, and the summary and discussions are given in Section 4.

2. Algorithm

Consider that a constellation, which is composed of $\mathrm{N} \geq 10$ spacecraft, performs in situ observations on a certain physical field f (density, magnetic field, or electric potential, etc.). In the Earth center frame of reference (or other inertial frames of the investigator), the Cartesian coordinates are (x^1, x^2, x^3) (corresponding to (x, y, z), respectively) with their bases ($\hat{\mathbf{x}}_1, \hat{\mathbf{x}}_2, \hat{\mathbf{x}}_3$). The position of the αth spacecraft is at

$x^i_{(\alpha)} = \left(x^1_{(\alpha)}, x^2_{(\alpha)}, x^3_{(\alpha)}\right)\left(\alpha = 1, 2, \cdots, N\right)$, and its velocity in the Earth center reference frame is $\mathbf{u}_{(\alpha)}$. The coordinates $x^{\mathrm{i}}_{\mathrm{c}}$ of the barycenter of the constellation satisfy

$$\sum_{\alpha=1}^{\mathrm{N}} \Delta x^{\mathrm{i}}_{(\alpha)} = \sum_{\alpha=1}^{\mathrm{N}} \left(x^{\mathrm{i}}_{(\alpha)} - x^{\mathrm{i}}_{\mathrm{c}}\right) = 0 . \tag{1}$$

So that

$$x^{\mathrm{i}}_{\mathrm{c}} = \frac{1}{\mathrm{N}} \sum_{\alpha=1}^{\mathrm{N}} x^{\mathrm{i}}_{(\alpha)} . \tag{2}$$

The physical quantity observed is $f'\left(x^i_\alpha\right) = f'_{(\alpha)}$ in the spacecraft reference frame and $f\left(x^i_\alpha\right) = f_{(\alpha)}$ in the Earth center reference frame (a static frame of reference), respectively. There is a certain transformation relationship between $f'_{(\alpha)}$ and $f_{(\alpha)}$. For the magnetic field, $\mathbf{B}'_{(\alpha)} = \mathbf{B}_{(\alpha)}$. For the electric field, $\mathbf{E}'_{(\alpha)} = \mathbf{E}_{(\alpha)} + \mathbf{u}_{(\alpha)} \times \mathbf{B}_{(\alpha)}$. For the electric and magnetic potentials, $\mathbf{A}'_{(\alpha)} = \mathbf{A}_{(\alpha)}$, $\phi'_{(\alpha)} = \phi_{(\alpha)} - \mathbf{u}_{(\alpha)} \cdot \mathbf{A}_{(\alpha)}$. For the charge density and current density, $\rho'_{(\alpha)} = \rho_{(\alpha)}$ and $\mathbf{j}'_{(\alpha)} = \mathbf{j}_{(\alpha)} - \mathbf{u}_{(\alpha)}\rho_{(\alpha)}$.

In the Earth center reference frame, the linear gradient of the physical quantity f is $\frac{\partial f}{\partial x^i} = \nabla_i f$, and its quadratic gradient is $\frac{\partial^2 f}{\partial x^i \partial x^j} = \nabla_i \nabla_j f$. Based on Taylor expansion, the physical quantity observed, $f_{(\alpha)}$, can be expressed as

$$f_{(\alpha)} = f_c + \Delta x^i_{(\alpha)} \nabla_i f_c + \frac{1}{2} \Delta x^i_{(\alpha)} \Delta x^j_{(\alpha)} \nabla_i \nabla_j f_c , \tag{3}$$

where all the gradients with orders higher than 2 are neglected under the assumption that $\Delta x^{\mathrm{i}}_{(\alpha)}$ are much less than the characteristic scale of the magnetic structures investigated. So that there are 10 parameters ($f_{\mathrm{c}}, (\nabla_i f)_c, (\nabla_i \nabla_j f)_c$) to be determined. The formula (3) can also be written as

$$f_{(\alpha)} = f_{\mathrm{c}} + \Delta x^i_{(\alpha)} \mathrm{g}_i + \frac{1}{2} \Delta x^i_{(\alpha)} \Delta x^j_{(\alpha)} \mathrm{G}_{ij} , \tag{3'}$$

where, the linear and quadratic gradients of the physical quantity at the barycenter are

$\mathrm{g}_i = (\nabla_i f)_c$ and $\mathrm{G}_{ij} = (\nabla_i \nabla_j f)_c$, respectively. It is noted that $\mathrm{G}_{ij} = \mathrm{G}_{ji}$. Therefore, to obtain the 10 parameters (f_c , g_i , G_{ij}), observations by the constellation with at least 10 spacecraft are required.

In order to obtain the estimator for the 10 parameters (f_c, g_i, G_{ij}) with the desired accuracy from the $\mathrm{N} \geq 10$ spacecraft in situ observations, we make use of the least square method (Harvey, 1998; Shen et al., 2003). Assume the action to be

$$S = \frac{1}{\mathrm{N}} \sum_{\alpha} \left[f_\mathrm{c} + \Delta x^i_{(\alpha)} \mathrm{g}_i + \frac{1}{2} \Delta x^i_{(\alpha)} \Delta x^j_{(\alpha)} \mathrm{G}_{ij} - f_{(\alpha)} \right]^2 . \tag{4}$$

Minimize it by

$$\delta S = 0 , \tag{5}$$

so as to find the formulas for f_c, $\mathrm{g}_i = (\nabla_i f)_c$ and $\mathrm{G}_{ij} = (\nabla_i \nabla_j f)_c$.

Equation (5) leads to

Due to

$$\begin{aligned} \frac{\partial S}{\partial f_\mathrm{c}} &= \frac{1}{\mathrm{N}} \sum_{\alpha=1}^{\mathrm{N}} 2 \left[f_c + \Delta x^i_{(\alpha)} \mathrm{g}_i + \frac{1}{2} \Delta x^i_{(\alpha)} \Delta x^j_{(\alpha)} \mathrm{G}_{ij} - f_{(\alpha)} \right] \\ &= 2 \cdot \frac{1}{\mathrm{N}} \sum_{\alpha=1}^{\mathrm{N}} \left[f_c - f_{(\alpha)} \right] + 2 \cdot \frac{1}{\mathrm{N}} \sum_{\alpha=1}^{\mathrm{N}} \Delta x^i_{(\alpha)} \mathrm{g}_i + \frac{1}{\mathrm{N}} \sum_{\alpha=1}^{\mathrm{N}} \Delta x^i_{(\alpha)} \Delta x^j_{(\alpha)} \mathrm{G}_{ij} = 0 \end{aligned} , \tag{7}$$

we get

$$f_\mathrm{c} = \frac{1}{\mathrm{N}} \sum_{\alpha} f_{(\alpha)} - \frac{1}{2N} \sum_{\alpha}^{\mathrm{N}} \Delta \mathrm{x}^\mathrm{i}_{(\alpha)} \Delta \mathrm{x}^\mathrm{j}_{(\alpha)} G_\mathrm{ij} , \tag{8}$$

where the equation (1) is used. The above equation can also be written as

$$f_c = \frac{1}{\mathrm{N}} \sum_{\alpha} f_{(\alpha)} - \frac{1}{2} \mathrm{R}^\mathrm{ij} G_\mathrm{ij} . \tag{8'}$$

Here R^{ij} is the volumetric tensor (or 3×3 matrix) (Harvey, 1998; Shen et al., 2003), which is defined as

$$R^{ij} \equiv \frac{1}{N}\sum_{\alpha=1}^{N}\Delta x^{i}_{(\alpha)}\Delta x^{j}_{(\alpha)} = \frac{1}{N}\sum_{\alpha=1}^{N}\left(x^{i}_{(\alpha)} - x^{i}_{c}\right)\left(x^{j}_{(\alpha)} - x^{j}_{c}\right). \tag{9}$$

Therefore, the physical quantity at the barycenter is the average of all the measurements plus the correction term by the quadratic gradient.

From $\partial S / \partial g_i = 0$, we get

$$\frac{\delta S}{\delta g_i} = \frac{1}{N}\sum_{\alpha=1}^{N}2\left[f_c - f_{(\alpha)} + \Delta x^{k}_{(\alpha)}g_k + \frac{1}{2}\Delta x^{k}_{(\alpha)}\Delta x^{m}_{(\alpha)}G_{km}\right]\Delta x^{i}_{(\alpha)}$$

$$= -2\cdot\frac{1}{N}\sum_{\alpha=1}^{N}f_{(\alpha)}\Delta x^{i}_{(\alpha)} + 2R^{ik}g_k + R^{ikm}G_{km} = 0, \tag{10}$$

where the 3 order tensor is defined as

$$R^{ikm} \equiv \frac{1}{N}\sum_{\alpha=1}^{N}\Delta x^{i}_{(\alpha)}\Delta x^{k}_{(\alpha)}\Delta x^{m}_{(\alpha)}. \tag{11}$$

R^{ikm} is symmetrical, i.e., $R^{ikm} = R^{kim} = R^{imk}$. Eq. (10) reduces to

$$R^{ik}g_k = \frac{1}{N}\sum_{\alpha}^{N}\left(x^{i}_{(\alpha)} - x^{i}_{c}\right)f_\alpha - \frac{1}{2}R^{ikm}G_{km}. \tag{12}$$

Let R^{-1} be the inverse of the volumetric tensor, which satisfies $\left(R^{-1}\right)_{ik}R^{kj} = R^{jk}\left(R^{-1}\right)_{ki} = \delta^{j}_{i}$. Hence the linear gradient at the barycenter is obtained from Eq. (12) as follows

$$g_i = \left(R^{-1}\right)_{ij}\cdot\frac{1}{N}\sum_{\alpha}^{N}\left(x^{j}_{(\alpha)} - x^{j}_{c}\right)f_\alpha - \frac{1}{2}\left(R^{-1}\right)_{ij}R^{jkm}G_{km}. \tag{13}$$

The second term at the right-hand side of the above formula is the correction arising from the quadratic gradient.

From $\partial S / \partial G_{ij} = 0$, we get

$$\frac{\partial \mathrm{S}}{\partial \mathrm{G}_{\mathrm{ij}}}=\frac{1}{\mathrm{N}}\sum_{\alpha=1}^{\mathrm{N}}\left[f_{\mathrm{c}}-f_{(\alpha)}+\Delta x_{(\alpha)}^{\mathrm{k}}\mathrm{g}_{\mathrm{k}}+\frac{1}{2}\Delta x_{(\alpha)}^{\mathrm{k}}\Delta x_{(\alpha)}^{\mathrm{m}}\mathrm{G}_{\mathrm{km}}\right]\Delta x_{(\alpha)}^{\mathrm{i}}\Delta x_{(\alpha)}^{\mathrm{j}}=0. \qquad (14)$$

Thus

$$f_{\mathrm{c}}\mathrm{R}^{\mathrm{ij}}-\frac{1}{\mathrm{N}}\sum_{\alpha=1}^{\mathrm{N}}f_{(\alpha)}\Delta x_{(\alpha)}^{\mathrm{i}}\,\Delta x_{(\alpha)}^{\mathrm{j}}+\mathrm{R}^{\mathrm{ijk}}\mathrm{g}_{\mathrm{k}}+\frac{1}{2}\mathrm{R}^{\mathrm{ijkm}}\mathrm{G}_{\mathrm{km}}=0, \qquad (15)$$

where the 4-order tensor

$$\mathrm{R}^{\mathrm{ijkm}}\equiv\frac{1}{\mathrm{N}}\sum_{\alpha=1}^{\mathrm{N}}\Delta x_{(\alpha)}^{\mathrm{i}}\Delta x_{(\alpha)}^{\mathrm{j}}\Delta x_{(\alpha)}^{\mathrm{k}}\Delta x_{(\alpha)}^{\mathrm{m}}. \qquad (16)$$

Note that $\mathrm{R}^{\mathrm{ijkm}}$ is symmetric with $\mathrm{R}^{\mathrm{ijkm}}=\mathrm{R}^{\mathrm{jikm}}=\mathrm{R}^{\mathrm{ijmk}}=\mathrm{R}^{\mathrm{kmij}}$. Obviously, f_c, $\mathrm{g}_i=(\nabla_i f)_c$ and $\mathrm{G}_{ij}=(\nabla_i\nabla_j f)_c$ can be obtained by solving the equations (8’)，(12) and (15).

In order to ensure the calculation accuracy, we perform iterations to solve these equations, which can be conveniently realized by computation. At first, the linear approximation is made with $\mathrm{G}_{ij}=0$. Therefore, from the formulas (8’) and (13)，we obtain the physical quantity and its linear gradient at the barycenter as

$$f_{\mathrm{c}}=\frac{1}{\mathrm{N}}\sum_{\alpha}f_{(\alpha)}, \qquad (17)$$

and

$$\mathrm{G}_{\mathrm{i}}=(\nabla_{\mathrm{i}}f)_{c}=\left(\mathrm{R}^{-1}\right)_{\mathrm{ik}}\cdot\frac{1}{\mathrm{N}}\sum_{\varepsilon}^{\mathrm{N}}\left(x_{(\alpha)}^{\mathrm{k}}-x_{c}^{\mathrm{k}}\right)f_{\alpha}, \qquad (18)$$

respectively. Secondly, by substituting the above two equations into (15)，we can get

$$\frac{1}{2}\mathrm{R}^{\mathrm{ijkm}}\mathrm{G}_{\mathrm{km}}=\frac{1}{\mathrm{N}}\sum_{\alpha=1}^{\mathrm{N}}f_{(\alpha)}\Delta x_{(\alpha)}^{\mathrm{i}}\,\Delta x_{(\alpha)}^{\mathrm{j}}-f_{\mathrm{c}}\mathrm{R}^{\mathrm{ij}}-\mathrm{R}^{\mathrm{ijk}}\mathrm{g}_{\mathrm{k}}, \qquad (19)$$

with which the quadratic gradient G_{km} at the zero-order can be attained. the zero-order quadratic gradient G_{km} into (8') and (13) to yield the physical quantity f_c at the second order and its linear gradient $g_i = (\nabla_i f)_c$ at the first order; and again by using Eq. (19) to get the corrected quadratic gradient G_{km} at the first order. Repeat the above processes, so as to yield the solutions of Eqs. (8'), (12) and (15), i.e., the estimations of the 10 parameters (f_c, $g_i = (\nabla_i f)_c$, $G_{ij} = (\nabla_i \nabla_j f)_c$) of the plasma structure investigated.

Equation (19) is a tensor equation, which concrete solution we need to find. Rewrite it as the following expression

$$\sum_{l=1}^{3}\sum_{k=1}^{3} R^{ijkl} G_{kl} = c^{ij}, \quad i, j = 1,2,3. \tag{20}$$

The tensor at the right-hand side of the above equation is defined as

$$c^{ij} \equiv \frac{2}{N}\sum_{\alpha=1}^{N} f_{(\alpha)} \Delta x^{i}_{(\alpha)} \Delta x^{j}_{(\alpha)} - 2 f_c R^{ij} - 2R^{ijk} G_k . \tag{21}$$

We will transform the tensor equation (20) into a matrix equation so as to obtain its solution concisely. The second-order tensor c^{ij} is symmetric, i.e., $c^{ij} = c^{ji}$. c^{ij} contains 6 independent components, which can be expressed as $c^{(ij)} = \left(c^{11}, c^{12}, c^{13}, c^{22}, c^{23}, c^{33}\right)$. Similarly, the symmetric underdetermined tensor G_{ij} also contains 6 independent components, which can be written as $G_{(ij)} = \left(G_{11}, G_{12}, G_{13}, G_{22}, G_{23}, G_{33}\right)$. The fouth-order tensor R^{ijkl} is symmetric, and $R^{ijkl} = R^{(ij)(kl)}$, where both ij and kl have six independent compositions. Therefore, the tensor equation (20) can be rewritten as

$$\sum_{l=k}^{3}\sum_{k=1}^{3} (2-\delta_{kl}) R^{ijkl} G_{kl} = c^{ij}, \quad (i = 1,2,3,\ j = i, \cdots, 3) \tag{22}$$

To facilitate the calculation, the coefficient at the left-hand side of the above equation should be index symmetric. Multiplying the two side of Eq. (22) by $(2-\delta_{ij})$ to yield

$$\sum_{l=k}^{3}\sum_{k=1}^{3}(2-\delta_{ij})(2-\delta_{kl})R^{ijkl}G_{kl}=(2-\delta_{ij})c^{ij},\quad (i=1,2,3,\ j=i,\cdots,3.) \tag{23}$$

Note that in the above formula the sum over the indices i and j are not made even if i and j are repeated. The formula (23) can be regarded as a matrix equation in a 6-dimensional space. The bases of this 6-dimensional space are ($\hat{\mathbf{X}}_1\hat{\mathbf{X}}_1,\hat{\mathbf{X}}_1\hat{\mathbf{X}}_2,\hat{\mathbf{X}}_1\hat{\mathbf{X}}_3,\hat{\mathbf{X}}_2\hat{\mathbf{X}}_2,\hat{\mathbf{X}}_2\hat{\mathbf{X}}_3,\hat{\mathbf{X}}_3\hat{\mathbf{X}}_3$), which can also be marked as $\left(\hat{\boldsymbol{k}}_1,\hat{\boldsymbol{k}}_2,\cdots,\hat{\boldsymbol{k}}_6\right)$, or $\hat{\boldsymbol{k}}_M$, M=1, 2, … , 6, satisfying $\hat{\boldsymbol{k}}_M\cdot\hat{\boldsymbol{k}}_N=\delta_{MN}$. The underdetermined tensor G_{ij}, which is composed of 6 independent components, can be treated as a vector in the 6-dimensional space and written as $\boldsymbol{G}=\left(X^1,X^2,\cdots,X^6\right)$ with its components

$$\boldsymbol{X}^M=\boldsymbol{G}_{(kl)}\,. \tag{24}$$

It can be expressed in vector format as

$$\boldsymbol{G}=\sum_{M=1}^{6}X^M\hat{\boldsymbol{k}}_M \tag{24'}$$

The term $(2-\delta_{ij})c^{ij}$ at the right-hand side of equation (23) is composed of 6 components, can also be regarded as a vector in the 6-dimensional space and expressed as $\boldsymbol{C}=\left(C^1,C^2,\cdots,C^6\right)$, with the components

$$C^M=(2-\delta_{ij})c^{(ij)}. \tag{25}$$

Thus the vector $\boldsymbol{C}$ in the 6-dimensional space is written as

$$\boldsymbol{C}=\sum_{M=1}^{6}C^M\hat{\boldsymbol{k}}_M\,. \tag{26}$$

At the same time, the coefficient tensor $(2-\delta_{ij})(2-\delta_{kl})R^{ijkl}$ can be treated as a 6×6 matrix：

$$\Re^{MN} \equiv (2-\delta_{ij})(2-\delta_{kl})R^{(ij)(kl)} \tag{27}$$

The index M corresponds to (ij), and N to (kl). The matrix $\Re^{MN}$ is symmetric and $\Re^{MN} = \Re^{NM}$. It can be expressed in vector format as

$$\Re = \Re^{MN}\hat{\boldsymbol{k}}_M\hat{\boldsymbol{k}}_N . \tag{28}$$

Just like the 3×3 volumetric matrix R^{ij}, the 6×6 matrix $\Re^{MN}$ respects the characteristic geometric features of the constellation.

Therefore, the tensor equation (20) has been transformed into a matrix equation as follows:

$$\Re^{MN}\cdot X^N = C^M , \tag{29}$$

which vector form is

$$\Re\cdot\mathbf{G} = \mathbf{C} . \tag{29'}$$

The symmetric matrix $\Re^{MN}$ can be diagonalized. Suppose that its eigenvectors are $\left(\hat{\boldsymbol{e}}_1,\hat{\boldsymbol{e}}_2,\cdots,\hat{\boldsymbol{e}}_6\right)$ with $\hat{\boldsymbol{e}}_M\cdot\hat{\boldsymbol{e}}_N = \delta_{MN}$, and its eigenvalues $\left(\Lambda_1,\Lambda_2,\cdots\cdots,\Lambda_6\right)$ with $\Lambda_1 \ge \Lambda_2 \ge \cdots \ge \Lambda_6 \ge 0$. The relationship between the eigenvectors $\left(\hat{\boldsymbol{e}}_1,\hat{\boldsymbol{e}}_2,\cdots,\hat{\boldsymbol{e}}_6\right)$ and the bases $\left(\hat{\boldsymbol{k}}_1,\hat{\boldsymbol{k}}_2,\cdots,\hat{\boldsymbol{k}}_6\right)$ is

$$\hat{\boldsymbol{e}}_M = \xi_{MN}\hat{\boldsymbol{k}}_N . \tag{30}$$

Then $\Re$ can be written as

$$\Re = \sum_{M=1}^{6}\Lambda_M\hat{\boldsymbol{e}}_M\hat{\boldsymbol{e}}_M . \tag{31}$$

In the eigenspace $\left(\hat{\boldsymbol{e}}_1,\hat{\boldsymbol{e}}_2,\cdots,\hat{\boldsymbol{e}}_6\right)$ of $\Re^{MN}$, $\boldsymbol{G}$ and $\boldsymbol{C}$ can be expressed as

$$\boldsymbol{G} = \sum_{M=1}^{6}\tilde{X}^M\hat{\boldsymbol{e}}_M , \tag{32}$$

and

$$\boldsymbol{C} = \sum_{M=1}^{6} \tilde{C}^{M} \hat{\boldsymbol{e}}_{M}\ , \tag{33}$$

Respectively.

Substituting (31), (32) and (33) into (29'), we get

$$\Lambda_M \tilde{X}^M \hat{\boldsymbol{e}}_M = \tilde{C}^M \hat{\boldsymbol{e}}_M\ . \tag{34}$$

Then

$$\Lambda_M \tilde{X}^M = \tilde{C}^M\ . \tag{35}$$

Thus

$$\tilde{X}^M = \frac{1}{\Lambda_M} \tilde{C}^M\ . \tag{36}$$

In the above formula, it is required that $\Lambda_L > 0$. If the eigenvalue $\Lambda_L = 0$, $\tilde{X}^L$ can not be determined.

Therefore,

$$\boldsymbol{G} = \sum_{M=1}^{6} \tilde{X}^M \hat{\boldsymbol{e}}_M = \sum_{M=1}^{6} \frac{1}{\Lambda_M} \tilde{C}^M \hat{\boldsymbol{e}}_M = \sum_{M,N=1}^{6} \frac{1}{\Lambda_M} \tilde{C}^M \xi_{MN} \hat{\boldsymbol{k}}_N \tag{37}$$

Comparing (32) and (37) leads to

$$X^N = \sum_{M,N=1}^{6} \frac{1}{\Lambda_M} \tilde{C}^M \xi_{MN}\ . \tag{38}$$

From (26), (30) and (33), we can get

$$\tilde{C}^M = \sum_{L}^{6} \xi_{ML} C^L\ . \tag{39}$$

Finally, the formula (38) becomes

$$X^N = \sum_{M,N,L}^{6} \frac{1}{\Lambda_M} \xi_{MN} \xi_{ML} C^L\ , \tag{40}$$

which is the solution for the 6 independent components of the quadratic gradient at the barycenter of the constellation in the Earth center reference frame.

In order to obtain a more accurate quadratic gradient, an iterative method is used. Correct the physical quantity f_c and its linear gradient $g_i = (\nabla_i f)_c$ at the barycenter by substituting the quadratic gradient G_{ij} attained from (40) into (8') and (13); Calculate the corrected tensor $\mathbf{C}^{\mathrm{ij}}$ by the expression (21); Further calculate the components of the 6-dimensional vector $\boldsymbol{C}$, $C^M = (2-\delta_{ij})c^{(ij)}$; Then get the components of the quadratic gradient at the barycenter, $\boldsymbol{X}^N = \boldsymbol{G}_{(kl)}$ from the formula (40), which have been corrected by the first iteration. Repeating the above cycle till satisfactory accuracy is achieved. This iteration method will be tested and its reliability verified in the next section.

The estimation of the quadratic gradient of a physical quantity relies on the configuration of the constellation. We can get the complete quadratic gradient if all the 6 eigenvalues of the characteristic matrix $\Re^{MN}$ are non-zero. However, as shown in the expression (40), the quadratic gradient can not be completely determined if one or more eigenvalues of the characteristic matrix $\Re^{MN}$ are zero. For example, if the constellation is linearly distributed, it can be seen from the definitions (16) and (27) that only the eigenvalue of the characteristic matrix $\Re^{MN}$ along the spacecraft array is larger than zero, while all the other 5 eigenvalues of the characteristic matrix $\Re^{MN}$ are equal to zero. Therefore, only the quadratic gradient along the spacecraft array can be attained in this situation. For the situation when the constellation is planar, the 3 eigenvalues of the characteristic matrix $\Re^{MN}$ along the directions in the spacecraft plane are larger than zero, while all the other 3 eigenvalues are zero. So that only the three components of the quadratic gradient in the constellation plane can be found.

For example, we can obtain the linear and quadratic gradients of the electric potential with this approach based on the $N \geq 10$ spacecraft potential measurements, and further get the electric field and charge density at the barycenter of the constellation. Suppose the electric potential observed at the position $\mathbf{r}_\alpha$ of the spacecraft α is $\phi_{(\alpha)} = \phi(\mathbf{r}_\alpha), \alpha = 1, 2, \cdots, \mathrm{N}$. By using the above algorithm, we can yield the electric potential ϕ_c and its linear and quadratic gradients, $(\nabla\phi)_c$ and $(\nabla^2\phi)_c$, at the barycenter of the constellation. Therefore, the electric field at the barycenter is

$$\mathbf{E} = -(\nabla\phi)_c . \tag{40}$$

With Gauss' law, we get the charge density at the barycenter as follows.

$$\rho = \varepsilon_0 (\nabla \cdot \mathbf{E})_\mathbf{c} = -\varepsilon_0 (\nabla^2\phi)_c . \tag{41}$$

As for the multiple spacecraft magnetic field measurements, thereby we can obtain the magnetic linear and quadratic gradients at the barycenter of the constellation, and further attain the complete geometry of the magnetic field lines (MFLs), including the Frenet frame, the curvature and torsion of the MFLs. Suppose that the magnetic field at the position $\mathbf{r}_\alpha$ of the spacecraft α is $\mathbf{B}_\alpha = \mathbf{B}(\mathbf{r}_\alpha), \alpha = 1,\ 2,\ \cdots,\ \mathrm{N}$. Utilizing the above algorithm, the magnetic field and its linear gradient $(\nabla\mathbf{B})_c = \nabla\mathbf{B}(\mathbf{r}_c)$ and quadratic gradient $(\nabla\nabla\mathbf{B})_c = \nabla\nabla\mathbf{B}(\mathbf{r}_c)$ at the barycenter of the constellation can be calculated. The tangential vector or the unit magnetic vector of the MFLs is $\hat{\mathbf{b}} = \mathbf{B}/B$. The curvature of the MFLs at the barycenter of the constellation can be estimated by the following formula [Shen et al., 2003；2020]

$$\kappa_{cj} = B_c^{-1} b_{ci} \left(\nabla_i B_j\right)_c - B_c^{-1} b_{ci} b_{cj} b_{cm} \left(\nabla_i B_m\right)_c . \tag{42}$$

The principal normal vector of the MFLs is $\hat{\mathbf{K}} = \boldsymbol{\kappa}/|\boldsymbol{\kappa}|$, and the binormal vector of the MFLs is $\hat{\mathbf{N}}=\mathbf{b}\times\hat{\mathbf{K}}$. From its definition, $\tau \equiv \dfrac{1}{\kappa}\dfrac{d^2\hat{\mathbf{b}}}{ds^2}\cdot\hat{\mathbf{N}}$, we can get the torsion of the MFLs at the barycenter of the constellation as the expression [Shen et al., 2020]

$$\tau_c = \kappa_c^{-1} B_c^{-3} N_{cj} B_{ci} \left(\nabla_i B_k\right)_c \left(\nabla_k B_j\right)_c + \kappa_c^{-1} B_c^{-3} N_{cj} B_{ck} B_{ci} \left(\nabla_k \nabla_i B_j\right)_c . \tag{43}$$

3. Tests

In this section, we will investigate the applicability of the algorithm to the vector field, and check its ability to yield the linear and quadratic magnetic gradients and the complete geometry of the magnetic field lines (MFLs) based on the multiple-points magnetic measurements.

The algorithm has been tested for the cylindrical force-free flux rope, dipole magnetic field and modeled geo-magnetospheric field, so as to evaluate its capability. 15-points measurements have been assumed. The tests are focused on how well the algorithm behaves as iterations are performed and how the truncation errors vary with the increase of relative measurement scale. Assuming L is the size of the constellation and D the local characteristic scale of the magnetic structure, the relative measurement scale is L/D. The influence of the number of spacecraft of the constellation on the truncation errors has also been analyzed.

3.1 Configuration of the constellation

The positions of the 15 spacecraft of the constellation in the barycenter coordinates are generated randomly, which are demonstrated in Figure 1. The three characteristic lengths of the constellation (Harvey, 1998) are $a = 0.75R_E, b = 0.61R_E, c = 0.24R_E$, respectively, and hence the size of the constellation is $L \equiv 2a = 1.5R_E$.

The elements of the 6×6 characteristic matrix $\Re^{MN}$ can be calculated by the definition (27), and its six eigenvalues are shown in Table 1. All of them are non-zero, thus the algorithm can be applied to calculate the linear and quadratic gradients with the measurements by this constellation. In the following tests, the configuration of the constellation will be kept unchanged, while its size adjusted by scaling up and down the distances between the spacecraft.

3.2 Flux ropes

The axially symmetric force-free flux rope will be used to test the algorethm developed in Section 2, the magnetic field in which in cylindrical coordinates can be expressed as (Lundquist, 1950)

$$\boldsymbol{B} = B_0[0, J_1(\alpha r), J_0(\alpha r)], \tag{44}$$

where r is the axial-centric distance, $1/\alpha$ the characteristic scale of the flux rope, J_n the first kind Bessel function of order n, and B_0 is the characteristic magnetic strength in the flux rope. We can set that $\alpha = 1/R_E$ and $B_0 = 60nT$. The overall spatial chracteristic scale of the flux rope is $D = 1/\alpha = 1R_E$. However, when $r < 1/\alpha = 1R_E$, it is proper to set the local characteristic scale as the axial-centric distance r, i.e., $D = r$. The helix angle β of the MFLs in the cylindrical flux rope obeys $\tan\beta = J_0(\alpha r)/J_1(\alpha r)$. The curvature and torsion of the MFLs are expressed as

$$\kappa = \mathrm{r}^{-1}\cos^2\beta \tag{45}$$

and

$$\tau = \kappa \tan\beta, \tag{46}$$

respectively [Shen, et al., 2020].

The linear and quadratic gradients ofthe magnetic field, $\nabla_\mathrm{i}\mathrm{B}_\mathrm{k}$ and $\nabla_\mathrm{i}\nabla_\mathrm{j}\mathrm{B}_\mathrm{k}$, are usually composed of 3*3=9 and 6*3=18 independent components, respectively. Axially symmetric flux rope has two symmetries: the three components of the magnetic field in the cylindrical coordinates are invariants along both the axial and azimuthal directions. So that some components of the quadratic magnetic gradient are zero. It is easy to find that, the 13 independent components of $\nabla_\mathrm{i}\nabla_\mathrm{j}\mathrm{B}_\mathrm{k}$ in Cartesian coordinates at one point of the x-axis are zero, i.e., $\partial_z\partial_i B_j = 0$, and $\partial_x\partial_x B_x = \partial_y\partial_y B_x = \partial_x\partial_y B_y = \partial_x\partial_y B_z = 0$; while the remaining 5 independent components, $\partial_x\partial_y B_x$, $\partial_x\partial_x B_y$, $\partial_y\partial_y B_y$, $\partial_x\partial_x B_z$ and $\partial_y\partial_y B_z$ are non-zero. Similarly, for the linear magnetic gradient, $\nabla_\mathrm{i}\mathrm{B}_\mathrm{j}$, its three components, $\partial_y B_x$, $\partial_x B_y$ and $\partial_x B_z$, are non-vanishing, and all the other 6 components are zero analytically. Without loss of generality, putting the barycenter of the constellation composed of 15 spacecraft at the x-axis, we can focus on checking the calculations of the algorithm on the 5 non-zero independent components of the quadratic magnetic gradient and 3 non-vanishing components of the linear magnetic gradient.

We first investigate the resultant's behavior during iterations. Assume that the barycenter of the constellation is at $[1,0,0]R_E$, and reduce the separations between the spacecraft of the constellation proportionally so that the relative measurement scale L/D$= 0.013$. We have performed the iterative calculation and tracked the errors of the linear and quadratic gradients of the magnetic field, which are plotted in Fig. 2. The relative error (vertical axis), $X_{algorithm}/X_{real} - 1$, before the first iteration is 1 since we assume these quantities vanished at the beginning (not shown in Fig.2). After the first iteration (horizontal axis), some of the relative errors have dropped under 0.3 while others remain high. With more iterations, the errors are decreasing and finally converge to certain fixed values as given by the exact solutions of the original equations. The number of iterations for the solutions to converge is varying and mostly less than 100. This has confirmed the convergence of the iteration method.

Secondly, we investigate the dependence of the truncation errors of the non-zero components of the linear and quadratic magnetic gradients on the relative measurement scale L/D.

We have tested three situations when the barycenter of the 15 spacecraft constellation are located at three representative points, [1,0,0] R_E, [0.5,0,0] R_E and

[0.1,0,0] R_E in Cartesian coordinates, respectively. We scale up and down the original 15-S/C constellation to adjust its characteristic size L. It is shown that, the algorithm yields reliable results for most relative measurement scale L/D.

The evaluation of calculations on the linear magnetic gradient and also the curvature of the magnetic field lines are made, which are illustrated in Figure 3(a),(c), and (e). The calculated linear magnetic gradient and curvature of the MFLs have sound accuracies and their relative errors are all less than 5%. As shown in Figure 3(a),(c), and (e), the relative errors of the three non-vanishing components of the linear magnetic gradient and the curvature of the magnetic field lines are varying at the second-order of L/D.

As shown in Figure 3(b),(d), and (f), the relative error (vertical axis) of the quadratic gradients (solid lines) increases about linearly with L/D (horizontal axis) and are generally less than 5 percent, so do that of the resultant torsion of the magnetic field lines (dashed and dotted lines) with slightly greater errors. Note that all errors shown in Fig.3 are converged. Such small errors imply that the algorithm runs well for the flux rope 15-point measurements.

Due to the magnetic field in the flux rope is generally varying rather slowly in space, the application of the algorithm on it is very effective and good accuracies can be reached as illustrated above. However, the magnetic field in space can have severe spatial variations, e.g., the dipole magnetic field. The strength of the dipolar magnetic field is decreasing by the third power of the distance from the dipole, and the magnetic gradients at every order are comparable. The actual calculations on the linear magnetic gradient and current density of the near-Earth magnetic field based on multiple spacecraft measurements are occasionally not accurate [Yang et al., 2016]. Here, we would like to apply the new algorithm to estimate the linear and quadratic magnetic gradients and check its accuracy and capability.

3.3 Dipole magnetic field

In this subsection, we will analyze the capability of the algorithm for the dipole magnetic field. The dipole field in Cartesian coordinates is assumed as

$$\boldsymbol{B} = \frac{M_z}{r^5}[3xy, 3yz, 3z^2 - r^2], \tag{47}$$

where M_z is the magnetic dipole moment and $r = \sqrt{x^2 + y^2 + z^2}$. It is supposed that the magnetic dipole moment points to the positive z-direction. the magnetic dipole moment is set as $M_z = -30438nT \cdot R_E^3$, which is approximately that of the Earth. It is easy to obtain the analytical expression of the curvature of the MFLs as

$$\kappa = \frac{3}{\mathrm{r}} \frac{\left(1+\cos^2\theta\right)\left|\sin\theta\right|}{\left(1+3\cos^2\theta\right)^{3/2}}, \tag{48}$$

where θ is the polar angle. The MFLs in the dipole magnetic field are plane curves, whose torsion is zero, i.e., $\tau = 0$.

The local characteristic scale D of the magnetic field measured can be chosen to be the distance of the constellation from the dipole, i.e., $\mathrm{D} = \mathrm{r}$.

The configuration of the constellation is the same as that in Subsection 3.1, which is shown in Figure 1. We scale up and down the original 15-S/C constellation to alter the characteristic size L of the constellation.

Firstly, we investigate the convergence behavior of the components of the linear and quadratic magnetic gradients calculated with the algorithm by iterations. The constellation is put at the equatorial plane of the dipole with its coordinates being $[3,0,0]\ R_E$, where only 5 independent components of the magnetic quadratic gradient are non-zero. The separations between the spacecraft of the constellation are reduced proportionally so that the relative measurement scale $L/D = 0.013$. The convergence behaviors of the non-vanishing independent components of the linear and quadratic magnetic gradients estimated by the algorithm are illustrated in Figure 4 (a) and (b), respectively, which indicates that the linear and quadratic magnetic gradients attain convergence within about 50 iterations.

Then the algorithm has been utilized to calculate the magnetic linear and quadratic gradients as well as the curvature and torsion of the MFLs in the dipole field as expressed by equation (47) for various characteristic scales of the constellation. The constellation is located at $[3,0,0], [2,0,3], [0,0,3]\ R_E$, respectively, which are corresponding to low, middle and high latitudes, respectively. Figure 5 (a,c,e) presents the relative errors of the calculated linear magnetic gradient and curvature of the magnetic field lines by the characteristic scale of the constellation. As shown in Figure 5 (a,c,e), the relative errors of the non-vanishing components of the linear magnetic gradient and the curvature of the magnetic field lines are of the second order of L/D.

As L/D< 0.01, the relative errors of the linear magnetic gradient are less than 5%. Therefore the linear magnetic gradient calculated has higher accuracy than the quadratic magnetic gradient. The variations of the relative errors of the magnetic quadratic gradient calculated with the algorithm by L/D are shown in Figure 5 (b,d,f). It can be seen that the relative errors of the magnetic quadratic gradient are at the first order in L/D. However, the errors in estimating the magnetic gradients are higher than those in the case of flux ropes. This is because that the dipolar magnetic strength is decreasing rather rapidly with the distance from the dipole. It is also shown in Figure 4 (b,d,f) that, as $L/D < 0.01$, the relative errors of the quadratic magnetic gradient are less than 10%.

3.4 Modeled Geomagnetosphere

By including one more dipole, the mirrored dipole, in the Earth's dipole field,

$$\boldsymbol{B} = \frac{M_{z1}}{r_1^5}[3xy, 3yz, 3z^2 - \mathrm{r}_1^2] + \frac{M_{z2}}{r_2^5}[3(x - 40R_E)y, 3yz, 3z^2 - \mathrm{r}_2^2], \quad (49)$$

the modeled geo-magnetospheric field is strongly inhomogeneous and continuously asymmetric, therefore serves as a scenario whereby the algorithm is tested more strictly and realistically. In Eq. (49), M_{z1} is the Earth's dipole moment, and $r_1 = \sqrt{x^2 + y^2 + z^2}$ the distance of the measurement point from the Earth's dipole. The mirror magnetic dipole, $M_{z2} = 28M_{z1}$, is located at $x = 40R_E$, and $r_2 = \sqrt{(x - 40R_E)^2 + y^2 + z^2}$ is the distance from the mirror dipole. In general, the modeled magnetospheric field is approximately equal to the Earth's dipole field in the inner region, $\mathrm{r}_1 \leq 6R_E$. Since the dipole field has been tested in the last subsection, we would focus on the outer region, $\mathrm{r}_1 > 6R_E$. Three points, [5, 15, 5] R_E, [5, 10, 10] R_E and [-5, 15, 10] R_E, corresponding to the far flank and high latitude at dayside and high latitude far flank at nightside, respectively, are chosen as the locations of the barycenter. Here we define the relative errors of the components $\partial_j B_i$ and $\partial_k \partial_j B_i$ as

$$e_{ij} = \frac{(\partial_j B_i)_{algorithm} - (\partial_j B_i)_{real}}{\langle \partial B \rangle}, \tag{50}$$

and

$$e_{ijk} = \frac{(\partial_k \partial_j B_i)_{algorithm} - (\partial_k \partial_j B_i)_{real}}{\langle \partial\partial B \rangle}, \tag{51}$$

respectively, where $\langle \partial B \rangle = \sum_{i,j}^{3} |\partial_j B_i| / 9$ and $\langle \partial\partial B \rangle = \sum_{i,j,k}^{3} |\partial_k \partial_j B_i| / 27$ are the average values of the components of linear and quadratic magnetic gradients, respectively. Figure 6 shows the convergent trend of the linear and quadratic gradients within 50 iterations when the separation between the spacecraft in the constellation is adjusted to make $L/D = 0.026$. Again the algorithm is confirmed to be reliable and suitable for analyzing fields severely varying in space.

Figure 7 illustrates the relative errors of all components of the linear and quadratic gradient calculated at different S/C scales. Due to the inhomogeneity and asymmetry of the geo-magnetospheric field, all components are non-vanishing. It is found that the linear gradients increase quadratically with L/D and quadratic gradients linearly with L/D. As $L/D < 0.01$, the relative errors of the quadratic gradient are below 10%, and those of the linear gradient below 5%. The accuracy of the algorithm for the modeled magnetospheric field is close to that for the dipole field.

The global geometry of the magnetospheric magnetic field can also serve as an elaborate scenario for testing. The geometrical features of the MFLs can be depicted by the curvature κ and torsion τ commonly. On the other hand, they can also be represented by another set of parameters, the radius of curvature and spiral angle, (R_c, β) [Apendix E in Shen, et al., 2020]. We have compared the analytical distributions of the radius of curvature and spiral angle of MFLs in $x = 0$ plane and those calculated based on the algorithm, and the results are as shown in figure 8 . Note that we have only modeled the region with （$y > 0, z > 0$）, one quarter of the magnetosphere, on considering the north-south and dawn-dusk symmetries of the modeled magnetosphere. Analytically, the modeled geomagnetic field has mirror symmetry about the z=0 coordinate plane (or the equatorial plane), so that the torsion of the MFLs is negated through the mirror and will be zero at the equatorial plane with z=0, as indicated in the panel (c) of Figure 8. The separation between the spacecraft is fixed to $L = 28km$. With the ever-changing D when we move the constellation around, the largest relative scale is$L/D = 0.0545$ at left-bottom corner (near the Earth), while the least scale $L/D = 0.00400$ at right-top corner. The raduis of curvature given by the algorithm is almost identical to its real value, as shown in the top panels of Figure (8).The MFLs tend to be more straight at the polar region and more bending at the low latitude region. The distribution of the spiral angle of the MFLs as attained by the algorithm is shown in Panel (d) of Figure (8), which is in good consistency with that analytically calculated as demonstrated in Panel (c). Both of them show the strong twist of the MFLs in the duskside cusp region. It is noted that at the low attitude polar region, the algorithm yields negative spiral angles of the MFLs, as shown in the deep blue area in Panel (d). This abnormal deviation from the accurate calculation mainly results from the extremely small curvature of the MFLs in this region.

In this test, 15 points measurements are applied and have verified the feasibility and accuracy of the algorithm. The algorithm needs at least 10 point measurements as input to estimate the quadratic gradient reliably. The more points the algorithm builds on, the more accurate the estimated quadratic gradients are.

To investigate this relationship, we need to exclude the effect of the spatial distribution of the constellation. For n points modeling, we have generated 1000 constellations spontanously, each of which consisting of n S/C, and then choose one constellation with minimum error of the calculation as the representative one. Figure 9 shows the mean relative errors of the linear and quadratic magnetic gradients at $[1,1,2]R_E$ in the modeled magnetospheric field derived from virtual measurements by constellations with different numbers of spacecraft, n, and two fixed characteristic spatial scales, L. As indicated by the dashed magenta lines, the mean error of the quadratic gradient is nearly proportional to $1/n$. The mean error of the linear-gradient, however, appears to be a constant plus a weak variation by the S/C number of the constellation. The averaged mean error of the linear magnetic gradient is about 2.07×10^{-1} as $L/D = 0.05$ and 8.28×10^{-3} as $L/D = 0.01$. As indicated from Figure 9, the results obtained here also confirm the previous arguments that the errors of the linear-gradient components decrease quadratically with L/D, and that of quadratic-gradient components linearly with L/D (see Fig. 9).

4 Summary and Conclusion

The algorithms for calculating the linear gradients of physical quantities based on the measurements by constellations composed of ≥4 spacecraft have been well established and found wide applications in Cluster, THEMIS and MMS data analyses. Recently a special algorithm for estimating the quadratic magnetic gradient utilizing the 4-point magnetic and particle observations has been developed and successfully applied in MMS data analysis [Shen et al. 2020]. With the evolution of space explorations, 10 or more S/C constellations can possibly be realized in the near future. Therefore it is meaningful to develop the method to draw the high order gradients of the physical quantities based on ≥10 point measurements so as to make well preparations for the future multiple point data analysis.

In this investigation, we have established the joint algorithm to deduce the linear and quadratic gradients of an arbitrary physical quantity by using the least square method. This approach can yield the linear and quadratic gradients at the barycenter of the constellation with the input of ≥10 point measurements. With the least square method, the equations for determining the physical quantity and its linear and quadratic gradients at the barycenter have been found. To solve these equations, iterations are made to find the approximation solutions. Firstly, under the linear approximation, the linear gradient is obtained from the multiple point measurements. Secondly, the quadratic gradient is calculated on these bases. Thirdly, the first iteration is made and the quantity and its linear gradient at the barycenter are modified with the obtained quadratic gradient. Then, the quadratic gradient is recalculated with the corrected values of the physical quantity and its linear gradient. The iterations are performed until the linear and quadratic gradients with satisfactory accuracies have been attained.

Generally, the determination of the 3 components of a physical quantity is dependent of the 3×3 volume matrix that reflects the configuration of the constellation. This exploration indicates that the calculations of the 6 independent components of the quadratic gradient rely on the 6×6 symmetric characteristic matrix $\Re^{MN}$ of the constellation. If the 6 eigenvalues of the characteristic matrix $\Re^{MN}$ are all nonzero, the 6 components of the quadratic gradient can be determined completely.

With the 10 point electric potential observations, the linear and quadratic gradients at the barycenter can be found, as well as the electric field and charge density. With the 10 point magnetic field measurements, the linear and quadratic magnetic gradients at the barycenter can be obtained, as well as the complete geometry of the magnetic field lines.

The tests on the algorithm have been made with the cylindrical flux ropes, dipole magnetic field and modeled geo-magnetospheric field, and the reliability and accuracy have been confirmed. In the test, the spatial distribution of the geometrical parameters (radius of the curvature and spiral angle) of the MFLs in the modeled geo-magnetospheric field has also been yielded, which are in well consistence with the analytic results. All the three tests show that, the calculations converge within 50 iterations. The attained linear gradient is at the second order accuracy, while the quadratic gradient at the first order accuracy. The test on the modeled geo-magnetospheric field indicates that increasing the number of the spacecraft in the constellation can enhance the accuracy of the quadratic gradient calculated and its relative errors are anti-proportional to the number of the S/C. However, the accuracy of the linear gradient yielded can not be further improved by increasing the number of the S/C, and its relative errors are almost independent of the number of the S/C. So that it is a very effective, reliable and accurate algorithm for jointly calculating the linear and quadratic gradients of various physical quantities with ≥10 point constellation measurements.

This approach can be used to calculate the complete geometrical parameters of the magnetic field (e.g., the curvature and torsion of the MFLs) in the magnetosphere (e.g., with T models) numerically. This algorithm is also very meaningful for the design of the future multiple S/C missions. For a constellation with 10 or more spacecraft, its characteristic matrix $\Re^{MN}$ needs to have six non-zero eigenvalues thus to make the complete determination of the quadratic gradients of the physical quantities possible. This algorithm will obviously find wide applications in the analysis of multiple point observation data.

Acknowledgments. This work was supported by National Natural Science Foundation (NSFC) of China Grant (No. 41874190, 41704168) and Shenzhen Technology Project (JCYJ20190806144013077). No observation data has been used in this investigation.

References

Chanteur, G. (1998), Spatial Interpolation for four spacecraft: Theory, in *Analysis Methods for Multi-Spacecraft Data*, edited by G. Paschmann and P. W.Daly, p. 349, ESA Publ. Div., Noordwijk, Netherlands.

De Keyser, J., Dunlop, M. W., Darrouzet, F., and D´ecr´eau, P. M. E.: Least-squares gradient calculation from multi-point observations of scalar and vector fields: Methodology and applications with Cluster in the plasmasphere, Ann. Geophys., 25, 971–987, 2007, http://www.ann-geophys.net/25/971/2007/.

Dunlop, M. W., D. J. Southwood, K.-H. Glassmeier, and F. M. Neubauer, Analysis of multipoint magnetometer data, Adv. Space Res., 8, 273, 1988.

Escoubet, C. P., Fehringer, M., & Goldstein, M. (2001), Introduction: The Cluster mission,*AnnalesGeophysicae*, *19*, 1197-1200,https://doi.org/10.5194/angeo-19-197-2001.

Harvey, C. C. (1998), Spatial gradients and the volumetric tensor, in *Analysis Methods for Multi-Spacecraft Data*, edited by G. Paschmann and P. W. Daly, p. 307, ESA Publications Division, Noordwijk, The Netherlands.

Lundquist, S. (1950). Magnetohydrostatic fields. Ark. Fys., 2, 361–365.

Russell, C. T., Anderson, B. J., Baumjohann, W., Bromund, K. R., Dearborn, D., Fischer, D., et al. (2016), The MagnetosphericMultiscale magnetometers,*Space Science Reviews, 199*(1-4), 189-256, https://doi.org/10.1007/s11214‐014‐0057‐3.

Shen, C., X. Li, M. Dunlop, Z. X. Liu, A. Balogh, D. N. Baker, M. Hapgood, and X.

Wang (2003), Analyses on the geometrical structure of magnetic field in the current sheet based on cluster measurements, *J. Geophys. Res.*, *108*(A5), 1168, doi:10.1029/2002JA009612.

Shen, C., C. Zhang, Z. J. Rong, Z. Y. Pu, M. Dunlop, C. P. Escoubet, C. T. Russell, G. Zeng, N. Ren, J. L. Burch, Y. F. Zhou (2020), The quadratic magnetic gradient and complete geometry of magnetic field lines deduced from multiple spacecraft measurements, *J. Geophys. Res.*, in submission.

Shue, J.-H., et al. (1998), Magnetopause location under extreme solar wind conditions, *J. Geophys. Res.*, *103*, 17,691, DOI: 10.1029/98JA01103.

Torbert, R. B., Dors, I., Argall, M. R., Genestreti, K. J., Burch, J. L., Farrugia, C. J., et al. (2020). A new method of 3‐D magnetic field reconstruction. Geophysical Research Letters, 47, e2019GL085542. https://doi.org/ 10.1029/2019GL085542.

Vogt, J., G. Paschmann, and G. Chanteur (2008), Reciprocal Vectors, in Multi-Spacecraft Analysis Methods Revisited, ISSI Sci. Rep., SR-008, edited by G. Paschmann and P. W. Daly, pp. 33–46, Kluwer Academic Pub., Dordrecht, Netherlands.

Vogt, J., A. Albert, and O. Marghitu (2009), Analysis of three-spacecraft data using planar reciprocal vectors: Methodological framework and spatial gradient estimation, Ann. Geophys., 27, 3249–3273, doi:10.5194/angeo-27-3249-2009.

Yang, Y. Y., C. Shen, M. Dunlop, Z. J. Rong, X. Li, V. Angelopoulos, Z. Q. Chen, G. Q. Yan, and Y. Ji (2016), Storm time current distribution in the inner equatorial magnetosphere: THEMIS observations, J. Geophys. Res. Space Physics, 121, doi:10.1002/ 2015JA022145.

Table 1: Eigenvalues (in R_E^4) of the characteristic matrix $\Re^{MN}$

Λ_1	Λ_2	Λ_3	Λ_4	Λ_5	Λ_6
0.03512	0.02385	0.002728	0.008468	0.01130	0.01080

Figure Captions

Figure 1: Schematic view of the distribution of the constellation.

Figure 2: The relative errors of the non-vanishing components of the linear (a) and quadratic (b) magnetic gradients in the flux rope calculated by different numbers of iterations. It is noted that $B_{i,k} = \partial B_i / \partial x_k$, $B_{i,j,k} = \partial^2 B_i / \partial x_j \partial x_k$, where a comma denotes partial differentiation.

Figure 3: Left panels (a),(c), and (e) show the relative errors of three non-vanishing components of the linear magnetic gradient and curvature (κ) of the magnetic field lines in flux rope by L/D calculated for three different locations of the constellation, [1,0,0] R_E, [0.5,0,0] R_E and [0.1,0,0] R_E in Cartesian coordinates, respectively. Right panels (b),(d), and (f) illustrate the relative errors of non-vanishing components of the quadratic magnetic gradient and torsion (τ) of the magnetic field lines in flux rope by L/D calculated for the three different locations of the constellation, [1,0,0] R_E, [0.5,0,0] R_E and [0.1,0,0] R_E in Cartesian coordinates, respectively.

Figure 4: The relative errors of the non-vanishing components of the linear (left panel (a)) and quadratic (right panel (b)) magnetic gradient in the dipole field at the equatorial plane as calculated by different numbers of iterations.

Figure 5: Left panels (a), (c) and (e) show the relative errors of the three non-vanishing components of the linear magnetic gradient and curvature (κ) of the MFLs in the dipole field by L/D calculated for three different locations of the constellation, [3, 0, 0] R_E, [2, 0, 3] R_E and [0, 0, 3] R_E in Cartesian coordinates, respectively. Right panels (b),(d), and (f) illustrate the relative errors of the non-vanishing components of the quadratic magnetic gradient in dipole field by L/D calculated for the three different locations of the constellation, [3, 0, 0] R_E, [2, 0, 3] R_E and [0, 0, 3] R_E in Cartesian coordinates, respectively.

Figure 6: The relative errors of the components of the linear (left panel (a)) and quadratic (right panel (b)) magnetic gradients in the modeled geomagnetic field at the position [-5, 15, 10] R_E as calculated by different numbers of iterations, the scale of the constellation is set as $L/D = 0.026$. In panel (b), dashed, dotted and solid lines with colors are for derivatives of B_1, B_2 and B_3 , respectively.

Figure 7: Left panels (a), (c) and (e) demonstrate the relative errors of the components of the linear magnetic gradient and curvature (κ) of the MFLs in the geomagnetic field by L/D calculated for three different locations of the constellation, [-5, 15, 10] R_E, [5, 10, 10] R_E and [5, 15, 5] R_E in Cartesian coordinates, respectively. The black dash-dotted line is for the curvature. Right panels (b), (d) and (f) illustrate the relative errors of the components of the quadratic magnetic gradient and torsion (τ) of the

MFLs in dipole field by L/D calculated for the three different locations of the constellation, [-5, 15, 10] R_E, [5, 10, 10] R_E and [5, 15, 5] R_E in Cartesian coordinates, respectively. The black dotted line is for the torsion.

Figure 8: Distributions of the radius of curvature (top) and helix angle (bottom) of MFLs in the coordinate plane x=0 in modeled magnetosphere based on theoretical (left) and new algorithm (right) calculations. The dashed line indicates the magnetopause when $B_z = 27nT, D_p = 3nPa$ [Shue et al., 1998].

Figure 9: Mean truncation errors of linear (red) and quadratic (blue) gradients for different numbers of measurement points. The modeling is for $L/D = 0.05$ (left) and $L/D = 0.01$ (right) at $[1,1,2]R_E$ in the modeled magnetosphere. The dashed magenta line is a fitted curve.

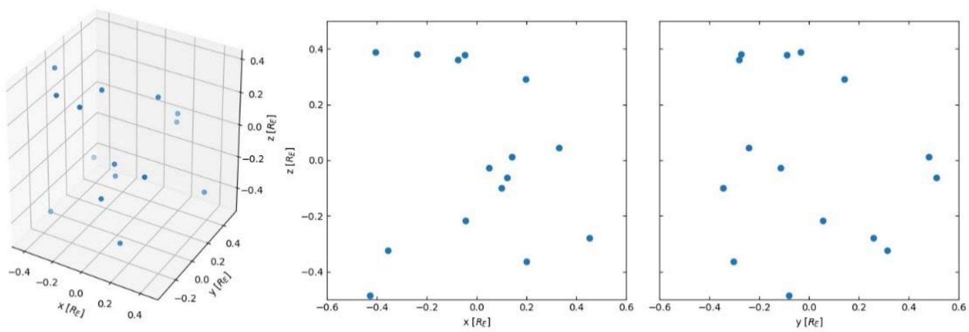

Figure 1: Schematic view of the distribution of the constellation.

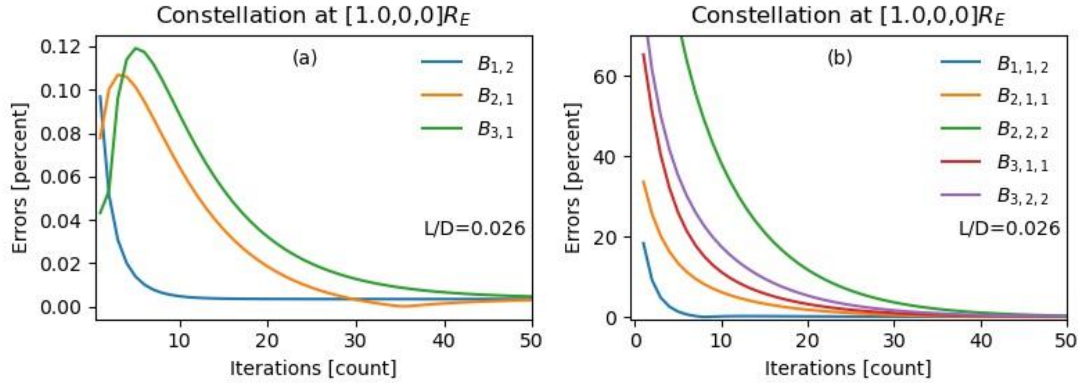

Figure 2: The relative errors of the non-vanishing components of the linear (a) and quadratic (b) magnetic gradients in the flux rope calculated by different numbers of iterations. It is noted that $B_{i,k} = \partial B_i / \partial x_k$, $B_{i,j,k} = \partial^2 B_i / \partial x_j \partial x_k$, where a comma denotes partial differentiation.

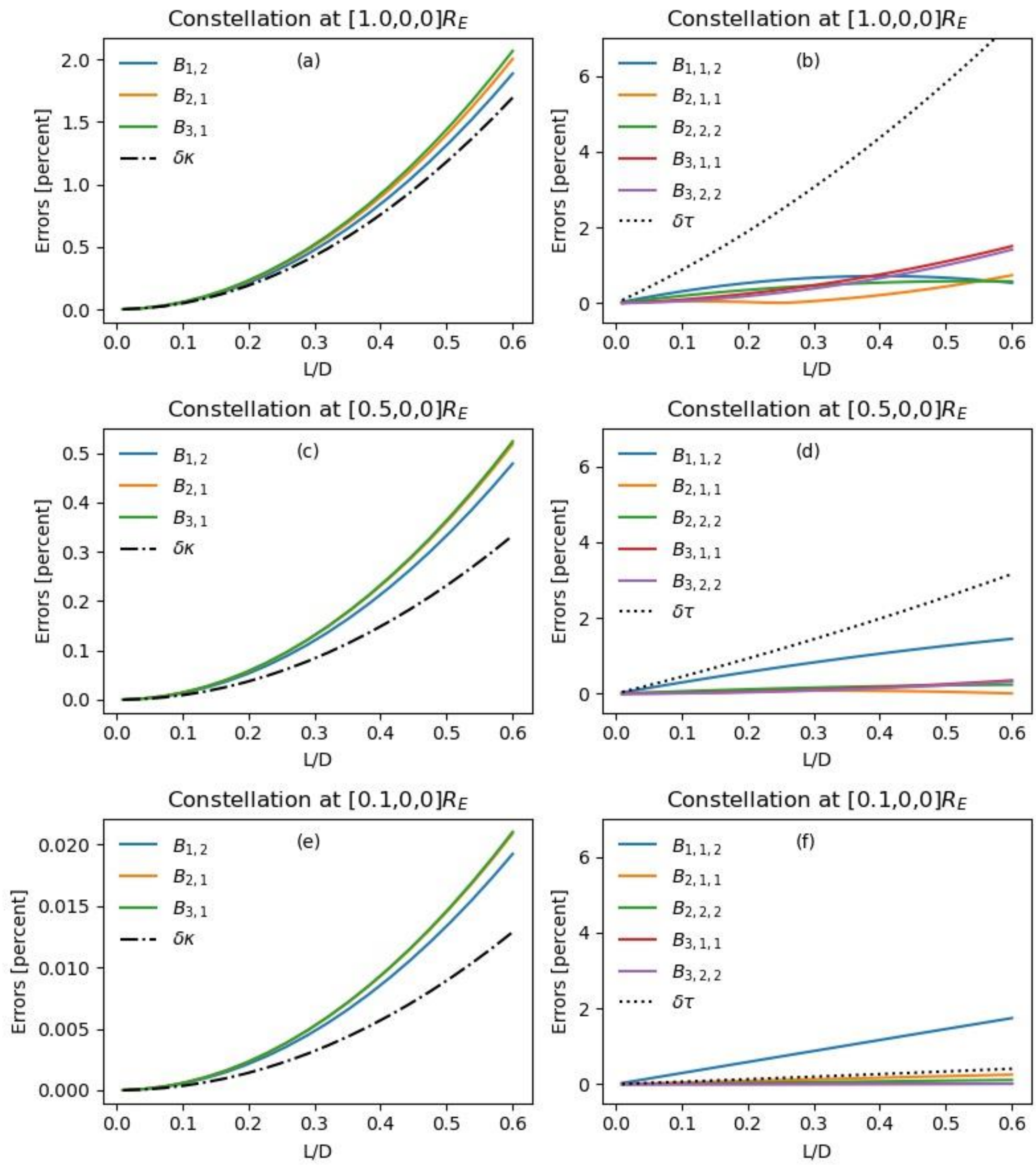

Figure 3: Left panels (a),(c), and (e) show the relative errors of three non-vanishing components of the linear magnetic gradient and curvature (κ) of the magnetic field lines in flux rope by L/D calculated for three different locations of the constellation, [1,0,0] R_E, [0.5,0,0] R_E and [0.1,0,0] R_E in Cartesian coordinates, respectively. Right panels (b),(d), and (f) illustrate the relative errors of non-vanishing components of the quadratic magnetic gradient and torsion (τ) of the magnetic field lines in flux rope by L/D calculated for the three different locations of the constellation, [1,0,0] R_E, [0.5,0,0] R_E and [0.1,0,0] R_E in Cartesian coordinates, respectively.

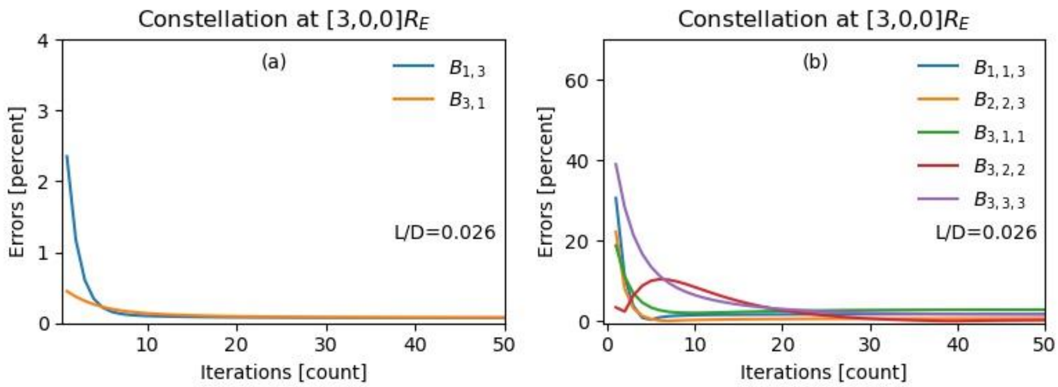

Figure 4: The relative errors of the non-vanishing components of the linear (left panel (a)) and quadratic (right panel (b)) magnetic gradient in the dipole field at the equatorial plane as calculated by different numbers of iterations.

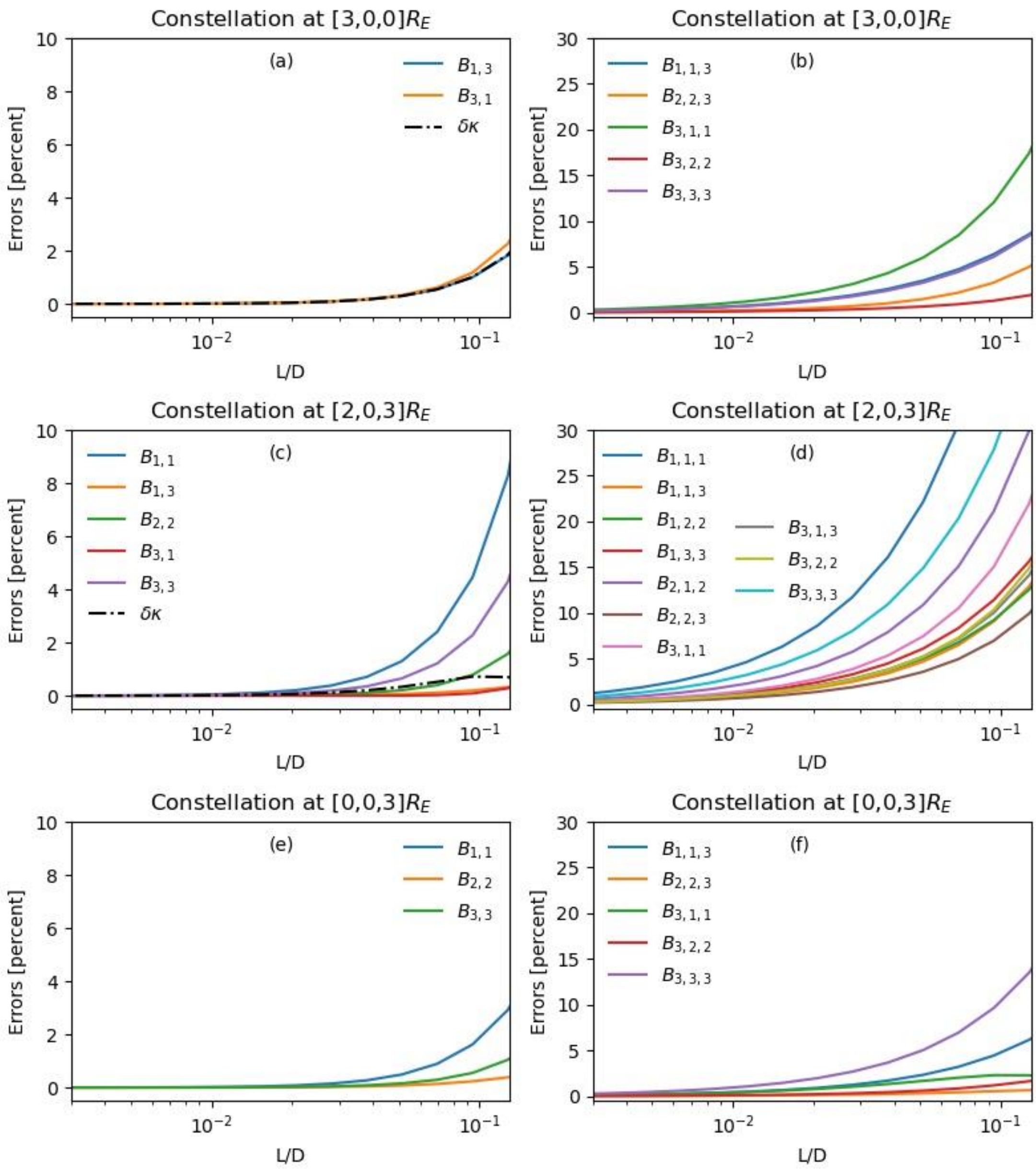

Figure 5: Left panels (a), (c) and (e) show the relative errors of the three non-vanishing components of the linear magnetic gradient and curvature (κ) of the MFLs in the dipole field by L/D calculated for three different locations of the constellation, [3, 0, 0] R_E, [2, 0, 3] R_E and [0, 0, 3] R_E in Cartesian coordinates, respectively. Right panels (b),(d), and (f) illustrate the relative errors of the non-vanishing components of the quadratic magnetic gradient in dipole field by L/D calculated for the three different locations of the constellation, [3, 0, 0] R_E, [2, 0, 3] R_E and [0, 0, 3] R_E in Cartesian coordinates, respectively.

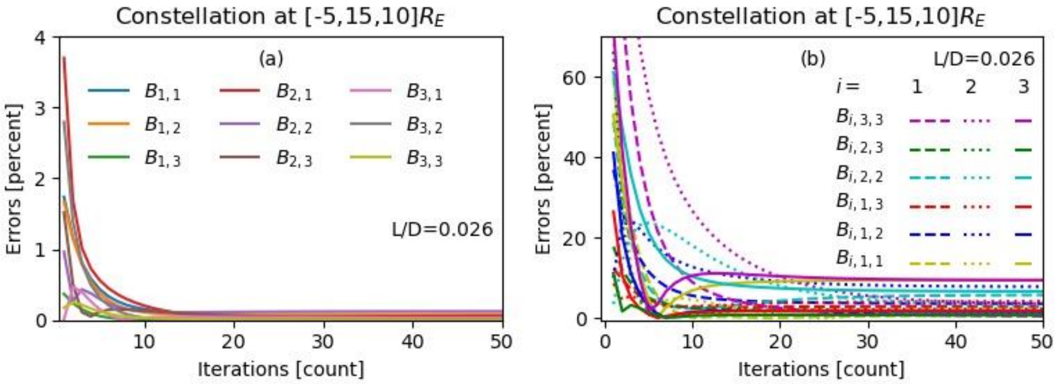

Figure 6: The relative errors of the components of the linear (left panel (a)) and quadratic (right panel (b)) magnetic gradients in the modeled geomagnetic field at the position [-5, 15, 10] R_E as calculated by different numbers of iterations, the scale of the constellation is set as $L/D = 0.026$. In panel (b), dashed, dotted and solid lines with colors are for derivatives of B_1, B_2 and B_3, respectively.

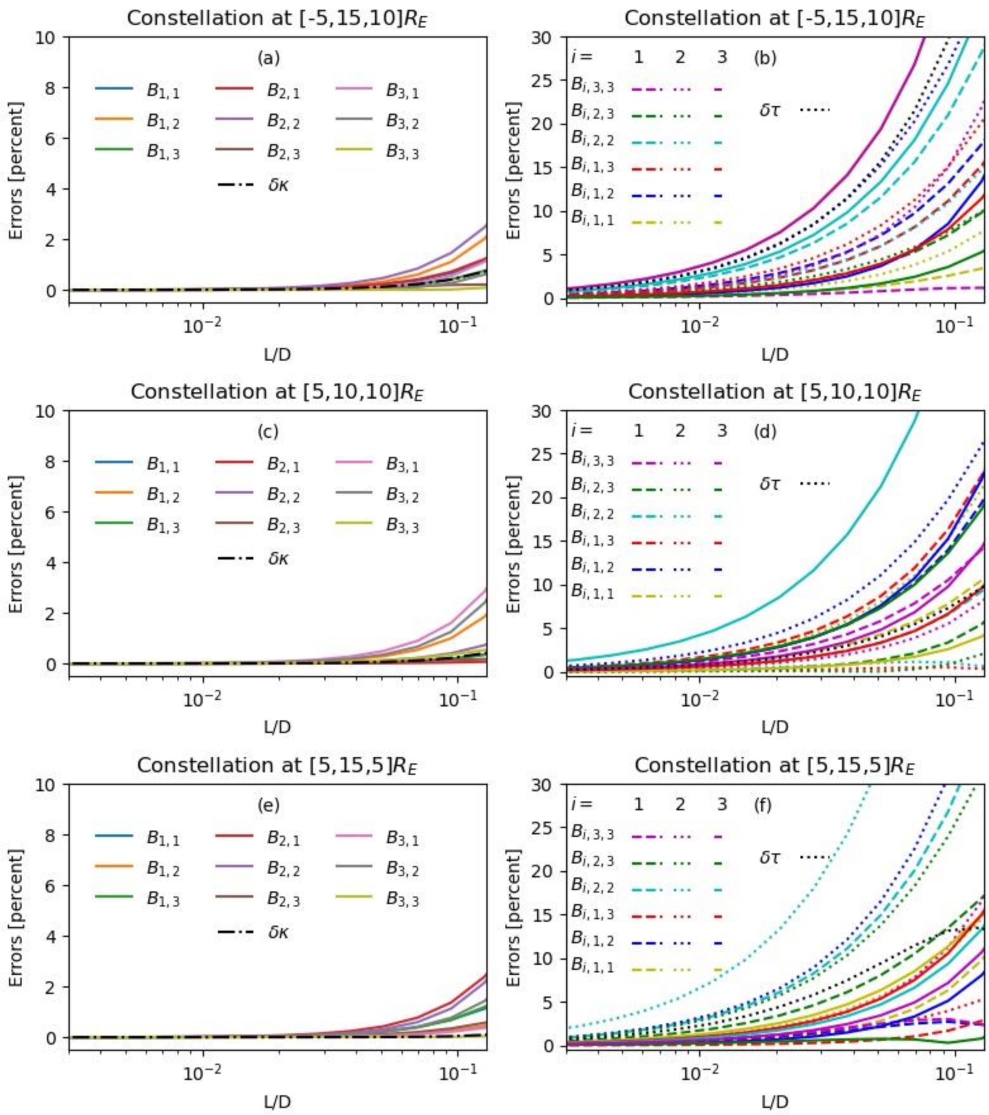

Figure 7: Left panels (a), (c) and (e) demonstrate the relative errors of the components of the linear magnetic gradient and curvature (κ) of the MFLs in the geomagnetic field by L/D calculated for three different locations of the constellation, [-5, 15, 10] R_E, [5, 10, 10] R_E and [5, 15, 5] R_E in Cartesian coordinates, respectively. The black dash-dotted line is for the curvature. Right panels (b), (d) and (f) illustrate the relative errors of the components of the quadratic magnetic gradient and torsion (τ) of the MFLs in dipole field by L/D calculated for the three different locations of the constellation, [-5, 15, 10] R_E, [5, 10, 10] R_E and [5, 15, 5] R_E in Cartesian coordinates, respectively. The black dotted line is for the torsion.

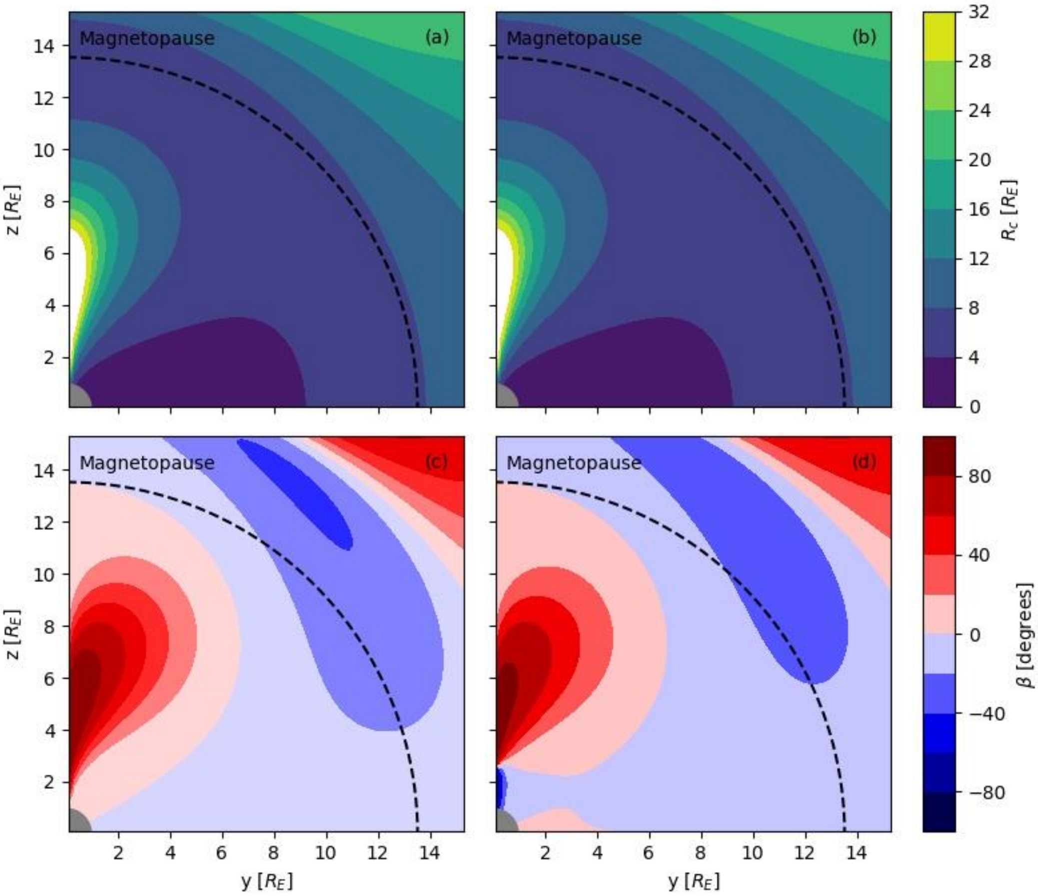

Figure 8: Distributions of the radius of curvature (top) and helix angle (bottom) of MFLs in the coordinate plane x=0 in modeled magnetosphere based on theoretical (left) and new algorithm (right) calculations. The dashed line indicates the magnetopause when $B_z = 27nT, D_p = 3nPa$ [Shue et al., 1998].

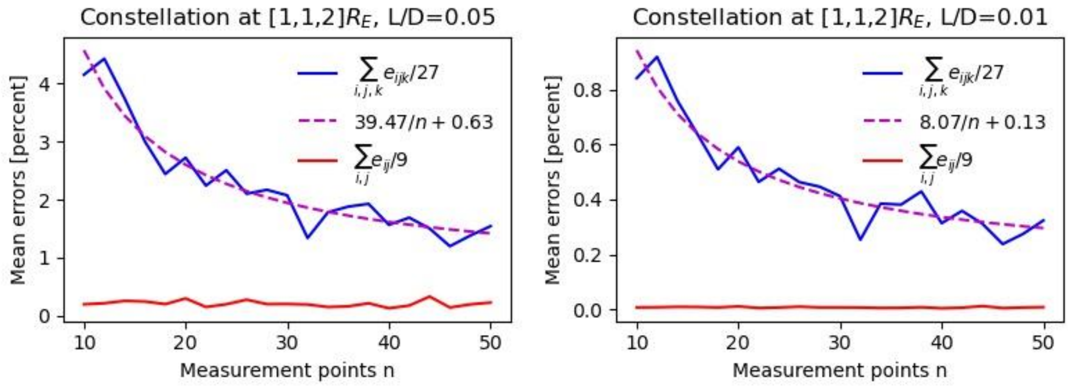

Figure 9: Mean truncation errors of linear (red) and quadratic (blue) gradients for different numbers of measurement points. The modeling is for $L/D = 0.05$ (left) and $L/D = 0.01$ (right) at $[1, 1, 2]R_E$ in the modeled magnetosphere. The dashed magenta line is a fitted curve.